# Properties and classification of enantiomerization pathways

Yariv Pinto, Yair Salomon and David Avnir

*Institute of Chemistry and The Lise Meitner Minerva Center for Computational Quantum Chemistry,*
*The Hebrew University of Jerusalem, Jerusalem 91904, Israel*
E-mail: david@chem.ch.huji.ac.il

Enantiomerization and automerization pathways are analyzed quantitatively using the continuous chirality measures methodology. The analysis gives rise to a number of new concepts and new descriptive tools, including isochirality, chirality maps, phase maps of nearest achirality and non-handed chirality. These allow one to classify enantiomerization processes into chiral, achiral, isochiral and non-handed categories.

## 1.　Background

In a recent series of papers [19–21] we advanced the notion that symmetry is a measurable structural quantity; we developed a methodology for the measurement of the degree of symmetry towards any symmetry group, including the important family of achiral groups [19]; and we demonstrated its applicability in a number of symmetry and chirality related issues [2,18]. These include the application of the symmetry measure as an order parameter in small clusters [3], an investigation of the chirality properties of the cyclic trimer of water and of its enantiomerization pathways [14], an analysis of the correlation between centrosymmetricity and hyperpolarizability [6], an analysis of the chirality of large random objects [1,7], an analysis of the enantiomerization properties of chiral fullerenes [13], implementation of continuous symmetry measures and continuous chirality measures in biomedical quantitative structure activity relations (QSAR) [8], and an analysis of the macroscopic chirality of tartrate crystals [9]. Major contribautions to the issue of measurement of chirality have been made by several research groups and a comprehensive listing of references can be found in [2,19].

In this paper we use the continuous chirality approach to explore in detail the properties of enantiomerization pathways and, in particular, of chiral pathways. Such pathways, in which all intermediate structures are chiral, are known and documented [10–12,15–17]. As is reported here, the *quantitative* exploration of it, which becomes possible with the chirality measure, allows one to define several novel concepts and descriptive tools, and to classify enantiomerization routes.

The specific example that accompanies our conceptual study is two-dimensional (2D) mainly for sake clarity of presentation; however, all the major conclusions reached

below hold for 3D-structures as well. Since the minimal number of vertices in 2D which allows chiral enantiomerization pathways is 4 [10,12], we selected to study the chirality properties of the simplest linearly connected 4 vertices structure in 2D, namely, a "butane-like" skeleton (figure 1(a)) (referred to in this report in short as "butane"). In order to get the entire picture of enantiomerization properties, full rotation is allowed around the two axes, as shown in figure 1(a). This object and its freedom of rotation are, of course, theoretical, but its simplicity allows one to present and discuss in a convenient way many of the properties of chirality in general. All chiral butane structures belong either to the 2D-$C_1$ point group or, in the case of equal $P_1 P_2$ and $P_3 P_4$ lengths, to the 2D-$C_2$ (=2D-inversion) point group, where $C_n$ is a point-axis of rotation within the plane. The achiral structures are either linear or cisoidal, having 2D-$C_s$ symmetry (figure 1 (b) and (c)) or, for the co-linear equal $P_1 P_2$ and $P_3 P_4$ lengths case (figure 1(d)), a 2D-$D_2$ symmetry. Finally, in declaring a structure chiral or not, we always retain the original connectivity, and therefore half-folded structures like figure 1(e) are chiral as well.

The continuous chirality measure (CCM) method we employ here is a special case of the more general continuous symmetry measures (CSM) approach. It has been described in detail in previous publications [2,18–21], and so we repeat here briefly only some elements needed for this report. Evaluating the chirality content of an object amounts by this approach to finding the minimal distance that the vertices of the object have to be shifted in order to attain achirality. It consists of three steps: normalization of the object size; applying a symmetry transform for finding the nearest achiral object; and calculation of the distance to the original structure, namely, the symmetry value.

The normalization is performed in order to make the CCM invariant to size and it is accomplished by division of all vertex distances of the object by the farthest distance from the center of mass. In center-of-mass coordinates, the locations of the vertices are

$$P_i = \frac{P_i^{\text{original}}}{P^{\text{farthest}}}. \tag{1}$$

In section 2.4 we propose an improved normalization procedure.

The symmetry transform is the heart of the CCM. It is based on dividing the vertices into matching (permutable) subgroups of vertices, folding the original normalized vertices $\{P_i\}$ within each of the subgroups, averaging the folded cluster and unfolding it into the normalized symmetric shape, $\{\widehat{P}_i\}$. The algorithm is demonstrated for $C_s$ in figure 2 (for details, see [19–21]). Once the set $\{\widehat{P}_i\}$ is obtained, the CCM value $S''(G)$ is calculated according to its definition:

$$S''(G) = \frac{1}{n} \sum_{i=1}^{n} \left| P_i - \widehat{P}_i \right|^2, \tag{2}$$

where $G$ is an achiral symmetry point group and $n$ is the number of vertices. This
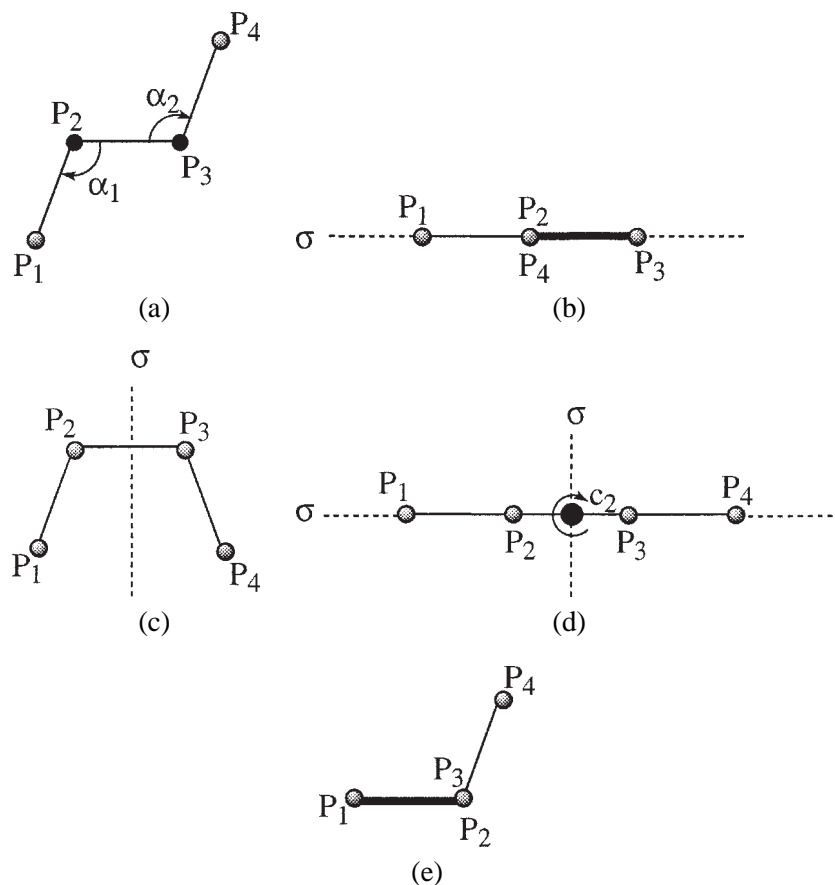
Figure 1. (a) The enantiomerizations are carried out on a two-dimensional (2D) chiral "butane-like" structure, by rotating the arms (vertices $P_1$ and $P_4$; the lengths need not be equal) around the axes $P_2$ and $P_3$. Full rotary motion as well as vertices overlap are allowed. Achiral shapes, which are also the nearest achiral structures to the chiral ones (see text for definition), are shown in (b)–(d). For the case of unequal bond lengths, the computed nearest achiral structures are those with all vertices collinear, either spread out or folded, such as in (b); or cisoidal structures (c) with $C_s$ symmetry. For the case of equal $P_1P_2$ and $P_3P_4$ lengths including the all-equal bond lengths, there is an additional type of nearest achiral structure: a linear butane with 2D-$D_2$ symmetry (d); shown are the two mirror lines and the $C_2$ axis. The vertices permutations (see text) for the three cases are: (b) (1)(2)(3)(4) – i.e., all vertices are reflected into themselves; (c) the pairs (1 4)(2 3) – i.e., $P_1$ is reflected into $P_4$, etc; and both permutations for (d).
  The half-folded structure (e) is chiral, because its original connectivity is retained.

procedure is repeated for every possible permutation (match) of vertices and for every (relevant) achiral point group, and the minimal value is chosen:

$$S'(G) = \min\left[S''(G)\right]_{\text{(over all the permutations)}} \qquad (3)$$

and

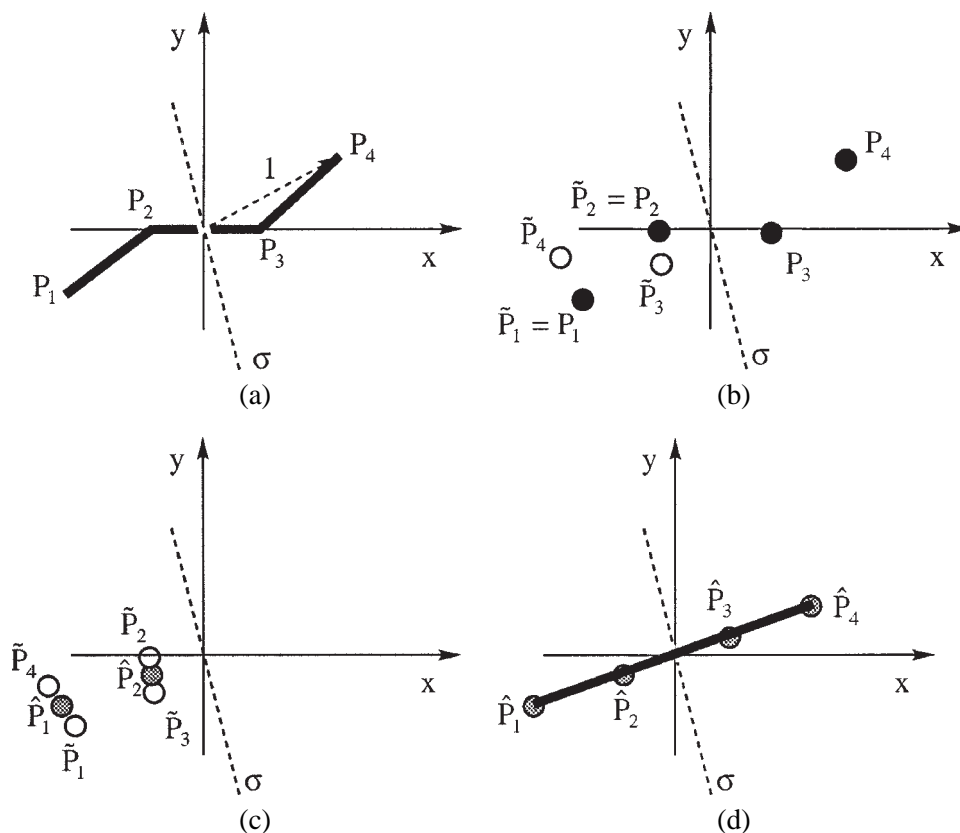$$S'(\text{chirality}) = \min\left[S'(G_{\text{improper}})\right]. \qquad (4)$$

Figure 2. The folding–unfolding method for evolution of the degree of chirality, demonstrated on a 2D butane. (a) The structure is placed so that its center of mass coincides with the origin, and its size normalized to unit size so that the maximal distance from the center of mass to the farthest point is 1. The points are paired (e.g., $P_1P_4$ and $P_2P_3$). The symmetry element, $\sigma$, is placed at the origin, and its optimal inclination (the one leading to minimal $S(G)$) is calculated analytically [19]. (b) The points are folded by applying the inverse symmetry operation on them: $e^{-1} \equiv e$ is operated on points $P_1$ and $P_2$; $\sigma^{-1} \equiv \sigma$ operates on $P_3$ and on $P_4$, producing the folded set of points, $\{\widetilde{P}_i\}$. (c) This set is averaged according to the permutation ($\widetilde{P}_1$ is averaged with $\widetilde{P}_4$ and $\widetilde{P}_2$ is averaged with $\widetilde{P}_3$), resulting in $\widehat{P}_1$ and $\widehat{P}_2$. (d) The averaged set is unfolded by operating the symmetry operations on the points, yielding the symmetrized set $\{\widehat{P}_i\}$. The chirality content is represented by the distance (squared) of (a) from (d), calculated from equation (6). This procedure is repeated over all possible permutations and the minimal value is selected.

In 2D, the only symmetry groups of relevance to chirality are those containing a mirror line $C_s$ and so in 2D the CCM is

$$S'(\text{chirality}) = S'(C_s). \qquad (5)$$

The minimal chirality value, $S'$, is zero for an achiral structure (and therefore, strictly speaking, $S'$ measures the distance from achirality). The maximal value of $S'(G)$ is 1 due to the normalization procedure, and it is obtained for some of the cases where

the nearest symmetric object is the center point [20,21]. For 2D-chirality it never reaches 1, because the distance to the mirror line is always smaller than the distance to a center point. Finally, we found it convenient to expand the scale by a factor of 100,

$$S(G) = 100 \cdot S'(G), \tag{6}$$

and these are the values reported here.

## 2.    Results and discussion

### 2.1.  *Achiral versus chiral enantiomerization and automerization routes: Qualitative aspects*

We first comment on the general butane structure, in which the three bond segments are of different length (representing, for instance, a C–C central bond with two different substituents on it). Allowing free rotations about the two axes ($P_2$ and $P_3$ in figure 1(a)), there are many possible enantiomerization routes, some achiral but mostly chiral. In general, as mentioned above, achirality is possible here only for co-linear structures, due to either full spreading ($\alpha_1 = \alpha_2 = 180°$), full folding ($0° = 360°$ for both angles) or a combination of both spreading and folding. A chiral enantiomerization pathway is therefore any route which does not pass through co-linearity.

We return to the generalized butane in section 2.3, and at the moment concentrate on a butane structure of equal segment lengths, with $\alpha_1 = \alpha_2 = 109.5°$, which, being a trans structure of $C_2$ symmetry, is chiral in 2D. Its enantiomer has bond angles of $360 - \alpha_1 = 360 - \alpha_2$ (figure 3, structures $I$ and $\overline{I}$). Achirality is achieved here, as in the generalized butane, when all vertices are co-linear. An achiral route passing through co-linearity is shown in figure 3(a). The route leading to it is a synchronous conrotatory motion of vertices $P_1$ and $P_4$. The higher symmetry of the $C_2$ butane allows additional achiral pathways: any pathway passing through an equal angles cis structure ($\alpha_1 = 360 - \alpha_2$, including, in fact, co-linearity) is an achiral pathway (figure 3(b)). Notice that all conrotatory pathways are achiral because these must pass through co-linearity or through a cis form. Disrotatory motion can lead, however, to both achiral and chiral pathways: chiral enantiomerization pathways are achieved here only by non-synchronous motion in which one of the end vertices passes over the 2–3 bond (figure 3 (c) and (d)).

The same arguments hold for a third process, namely, the automerization reaction. Here, an enantiomer moves along a pathway which returns into its original structure and handedness. Examples are figure 3 (e) and (f) – chiral routes – and figure 3(g) which is an achiral one.

Pathways (g) and (h) are of special interest: in (g) the chirality value remains constant throughout the process; in (h) it is not trivial to assign handedness to the structures along it. We return to these two special paths in sections 2.2 and 2.3.
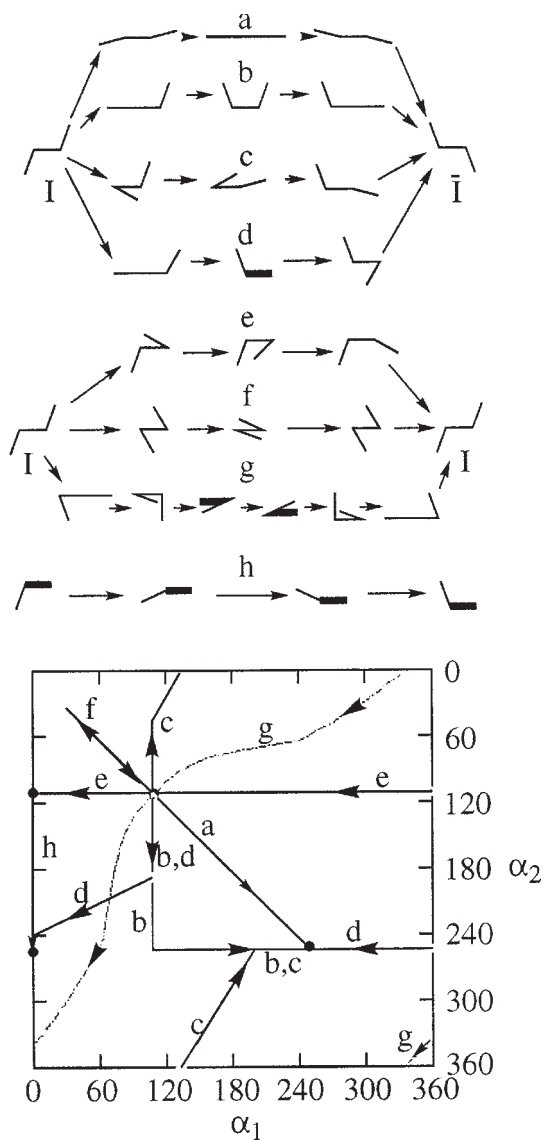
Figure 3. Top: (a)–(d) are enantiomerization pathways for a 2D butane skeleton of equal bond-lengths, which transform the structure $I$ to its enantiomer, $\bar{I}$. Representative structures along the pathways are shown. Path (a) is achiral and involves synchronous conrotatory clockwise motion of the arms. Path (b) is achiral as well, and involves stepwise conrotatory motion. (c) and (d) follow a non-synchronous disrotatory motion, leading to chiral pathways. Center: (e)–(g) are automerization pathways bringing $I$ back to itself. Path (e) is an achiral automerization and (g) and (f) are chiral ones. Path (g) (see section 2.2) represents an isochiral automerization route: the chirality value is constant throughout the process. Path (h) (see section 2.3) is an automerization of non-handed chirality. Bottom: the routes, from which the structures on top were taken, shown on an angles map. Note that the start and end points are the dots at 109.5° and that some routes cross the borders of the map and continue on the opposite side.

## 2.2. Quantitative representation of enantiomerization and automerization processes

The CCM methodology allows one to upgrade the qualitative description of section 2.1 to a quantitative level. Figure 4 shows the various routes described in figure 3 as $S$ versus reaction coordinate graphs. (The reaction coordinate is the actual route, shown in figure 3 (bottom), divided into equal segments.) It is seen that curves a, b, e and h pass through an achiral structure – the chirality value of these paths drops to zero at some point along the curve. The achiral entities for these paths are linear, cisoidal cisoidal and linear, respectively (figure 1). Curves c, d (enantiomerizations) and f, g (automerizations) represent chiral pathways, i.e., their $S$ values never drop to zero. Note (figure 4) that the CCM approach makes it possible to identify the most chiral structure in each of the routes (one of which is shown in the insert for curve f); and makes it possible to evaluate how much more (or less) chiral is any structure along the pathway, than the starting structure (e.g., the structure in the insert has a chirality value which is 4.85 times higher than the value of the starting shape).

The chiral paths give rise to interesting questions regarding handedness: where along the path does the handedness change? Are the points of change in handedness, which must be chiral themselves, unique in any way? What is the handedness of these chiral structures? We discuss these conceptual questions in a separate report and briefly in section 2.3. As mentioned above, another interesting pathway in figure 4 is represented by curve g. The chirality value throughout this process is constant – it is an *isochiral pathway* (figure 3(g)). The concept of *isochirality,* namely, structures possessing equal chirality values, is made possible, again, only by the use of quantitative measurement of chirality. Two identical structures or a pair of enantiomers are trivially isochiral, but also completely unrelated structures may be isochiral. In fact, if one draws a line in figure 4 which is parallel to the reaction coordinate, all the structures represented by the points where other graphs intersect it are isochiral. An example for such a line is curve g itself, which intersects some of the other curves and has therefore isochiral points with these curves. Other crossing points of other curves in figure 4 represent isochiral structures as well. In order to identify which of the crossing points represent different structures and which are trivially isochiral, it is necessary to analyse the angles maps (figure 3 (bottom)) or the chirality maps described in the next section, where we return to this point.

## 2.3. Chirality maps

So far we dealt with enantiomerization routes between mirror images of a specific butane structure of equal bond lengths and with $\alpha_1 = \alpha_2 = 109.5°$. However, isomerization pathways are possible between structures of *any* pair of angles, including, of course, isomerizations between butane structures of unequal angles. The CCM methodology allows one to present the chirality values of all possible structures, either in the form of chirality equicontour maps (figure 5(a)), or as a surface in a 3D-representation, shown in figure 5(b). As can be seen, the *chirality map* is quite rich in features such as valleys, ridges, saddles and so on. The highest points on this map, i.e., the most
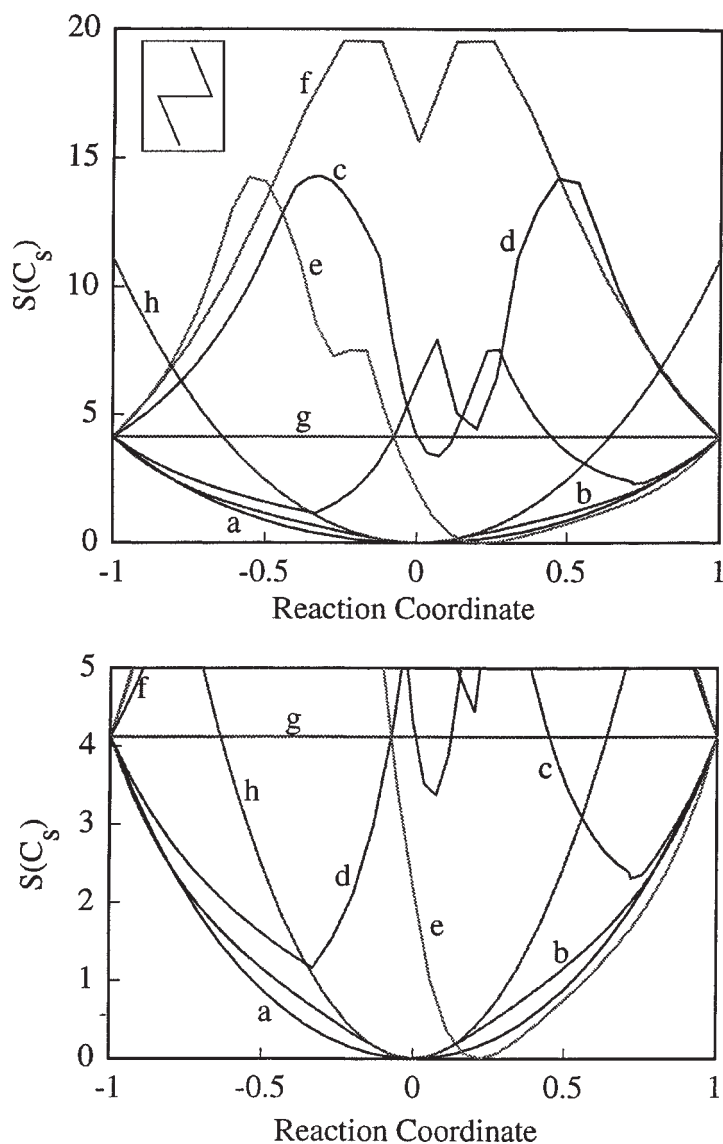
Figure 4. Variation of the chirality value throughout the reaction pathways shown in figure 3. Top: full picture. Bottom: enlarged detail. The reaction coordinate represents the trajectories in figure 3 (bottom) reduced into a line. Curves a and b are enantiomerization processes, passing through an achiral structure (chirality value zero), and so does the automerization curve e. Curves c and d represent chiral pathways in which the structure never becomes achiral, i.e., the $S$ value never drops to zero, as is the case for the automerization process f. Insert: the most chiral structure in the curve following route f has a chirality value of 20. Line g represents an isochiral process of constant $S$ value. The points of intersection between different routes represent isochiral structures. For section 2.3: curve h shows the $S$ variations along a non-handed route (following the dynamic rotational handedness definition in [5]). The achiral point ($S(C_s) = 0$) is trivially non-handed, yet all other points on this route represent chiral non-handed structures.
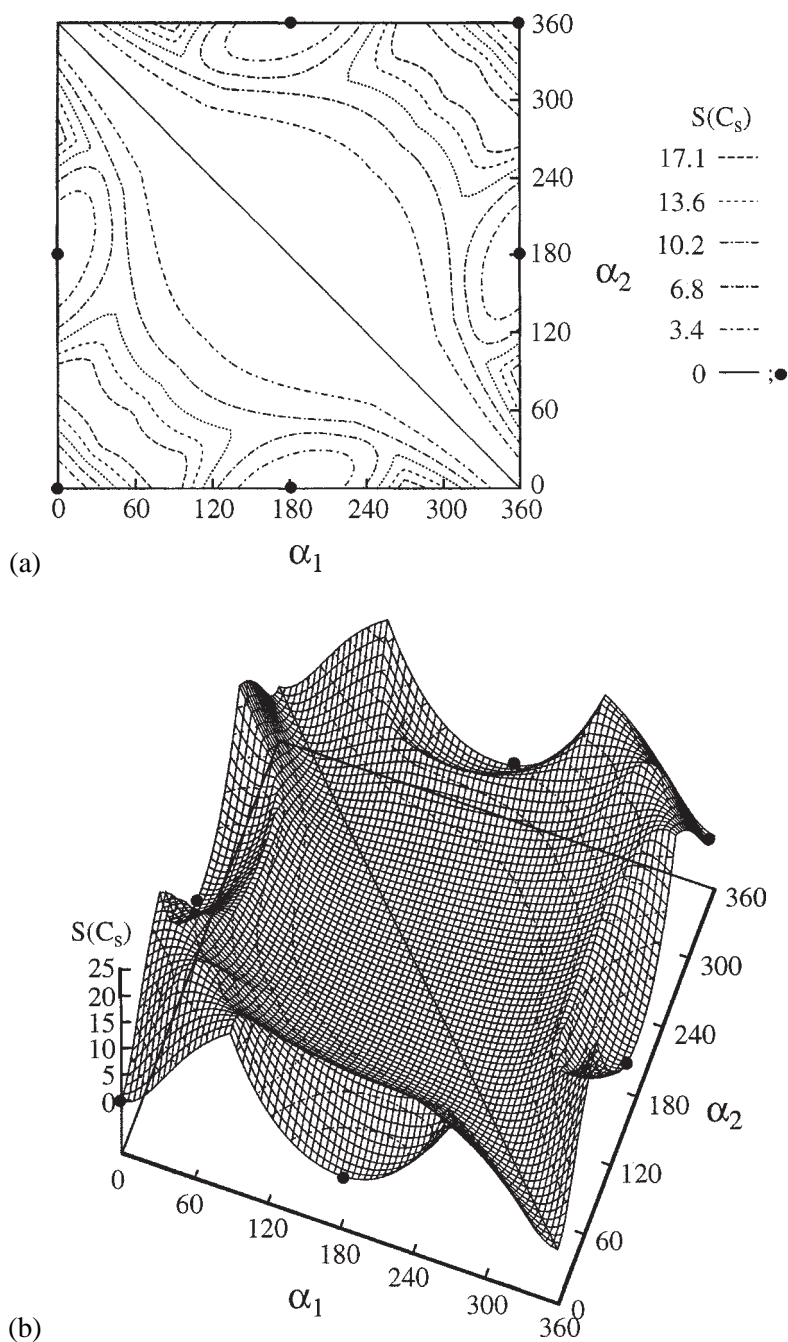
Figure 5. Chirality maps for butane structure of equal-bond lengths. The two ordinates are the angles defined in figure 1. (a) 2D-representation: contours of equi-chirality values. (b) 3D-representation of (a). Any two points (structures) on the map are connected by any of an infinite number of isomerization trajectories, the enantiomerizations of which are classified in the text.

chiral butane structures, are at (5,90), (90,5), (270,355) and (355,270) degrees. Their chirality value is 20.4. Chirality maps of butane structures with unequal bond lengths are discussed later in this section.

### 2.3.1. Classification of enantiomerization routes

The chirality map is a convenient tool for the full representation of the various enantiomerization routes, few examples of which were given in figure 3. In fact, any two structures on the chirality map are connected by an infinite number of isomerization routes. These can be classified as follows:

*Achiral isomerization routes.* An example of an isomerization route which is achiral in all its points, is the "valley" along the $\alpha_1 + \alpha_2 = 360°$ diagonal (figure 5) which corresponds to the $C_s$ symmetric cisoidal butane structures. All enantiomerization routes which cross this valley or pass along (portions of) it, or are tangents to it, are achiral routes. The same is of course true for automerization routes and in fact for any isomerization (namely, a reaction where the angles of starting structure and the angles of the end structure, are not equal). Another family of achiral routes are those which pass through the points $\alpha_1 = 0°$, $\alpha_2 = 180°$ or $\alpha_1 = 180°$, $\alpha_2 = 0°$, representing linear structures (the dots on the frame in figure 5).

*Chiral routes.* All routes which avoid the achiral diagonal valley ($\alpha_1 + \alpha_2 = 360°$) and the linear structures at the dots, are chiral. This means, as explained in section 2.1, that chiral enantiomerization pathways must pass through either of the $\alpha_i = 0°$ $(i = 1, 2)$ angles at least once; otherwise they have to pass the cisoidal achiral diagonal valley. (See figure 3 for some examples.)

*Isochiral routes.* We defined above isochirality as the property of having the same chirality *value*. The equicontours in figure 5(a) are, by definition, isochiral isomerization routes, along which the amount of chirality does not change. An example of how structures on such routes actually look like, was shown in figure 4 (curve g). As already discussed in our study of the enantiomerization of the water trimer [14], isochiral routes may be of particular interest: in that example, the energetically favored route is nearly isochiral. Closed loop isochiral contours represent isochiral automerizations. Completely achiral routes are isochiral routes with $S = 0$ all along the pathway, which, in our case, is the $\alpha_1 + \alpha_2 = 360°$ diagonal.

Different reaction pathways may cross each other in the chirality map (figure 3 (bottom)) and the points of crossing must, by definition, be isochiral (for instance, routes b and c). Obviously, isochirality at the points of crossing is of identical structures. However, reaction pathways, either crossing or not, may share isochiral structures which are located separately anywhere on the pathways. By and large, in such cases isochirality will be of different structures (see, for example, routes g and c). It should be noted again that the crossing of the curves in figure 4 indeed represent isochiral structures, but in order to identify which type it is, one has to resort to chirality maps (figures 3 and 5).

*Non-handed structures and routes.* An infinite number of chiral enantiomerization pathways exists for the butane structure (figure 5). Within each of these paths, the molecule changes its handedness without ever becoming achiral. This lead us to the notion that along the enantiomerization pathway, the structure must pass through a *non-handed* shape [14,21] – it is as left handed as it is right handed – yet still chiral. The specific shape of such non-handed structures depends on the handedness definition employed. For instance, the chiral half-folded shape, figure 1(e), is non-handed under the handedness definition suggested in [5]. The handedness assignment employed there is a dynamic rotational one: a chiral object (like figure 1(a)) is rotated in a viscous medium and, because of its chirality, the rotation creates more friction in the clockwise or in the counterclockwise direction. The difference between the two "friction" values is not only an additional measure of chirality but it also allows one to attach a sign to it and therefore also handedness. However, the chiral butane of figure 1(e) creates the same amount of friction in both directions of rotation, and therefore is non-handed under this handedness convention.[1] A trail of this type of non-handedness corresponds to $\alpha_1 = 0°$, $\alpha_2 \neq 0°$, $\alpha_2 \neq 180°$, or $\alpha_2 = 0°$, $\alpha_1 \neq 0°$, $\alpha_1 \neq 180°$ (the frame in figure 3). The phenomenon of non-handedness is conceptually interesting – we shall devote a separate report to its analysis.

### 2.3.2. The symmetry of chirality maps

Another telltale feature of the chirality maps is their symmetry. For the equal segments butane described in figures 3–5, the symmetry of the map (figure 5(a)) is 2D-$D_2$ ($C_{2v}$ in 3D). It is dictated by the symmetry of the linear structure at the middle point of the map ($\alpha_1 = \alpha_2 = 180°$) which also belongs to the 2D-$D_2$ symmetry point group. The reasoning behind the link between the symmetry of the map and the middle structure is that for every change in the shape of the latter, converting it to a structure anywhere else in the map, there are three other symmetry equivalent but re-positioned structures which retain the $D_2$ symmetry. Thus, a change of $+\Delta\alpha_1$ imposed on the linear center achiral structure, is equivalent to $-\Delta\alpha_2$ and enantiomeric to $-\Delta\alpha_1$ and $+\Delta\alpha_2$.

Chirality maps become more complex in features when one introduces different bond lengths (figure 6). However, the symmetry of the maps continues to obey the rule we just described, namely that the symmetry of full-spread collinear structure at the middle point dictates the symmetry of the whole map. In its most general form (all arms unequal to each other), the map itself is chiral, having a $C_2$ symmetry (2D inversion). To have this chiral symmetry, it suffices in fact to have unequal $P_1 P_2$ and $P_3 P_4$ bond lengths because the full spread structure is $C_s$ symmetric. For instance, figure 6(a) shows the map for bond lengths ratio of $1 : 1 : 2$. Its chiral $C_2$ symmetry is lower than the $D_2$ we encountered in figure 5(a), due to the lower symmetry of the center-point linear structure ($\alpha_1 = \alpha_2 = 180°$), namely, $C_s$ ($C_s$ and $C_2$ are isomorphic

---

[1] Thus, this method, although convenient and applicable to most structures, is not devoid of the problem of not identifying *all* chiral structures as such.
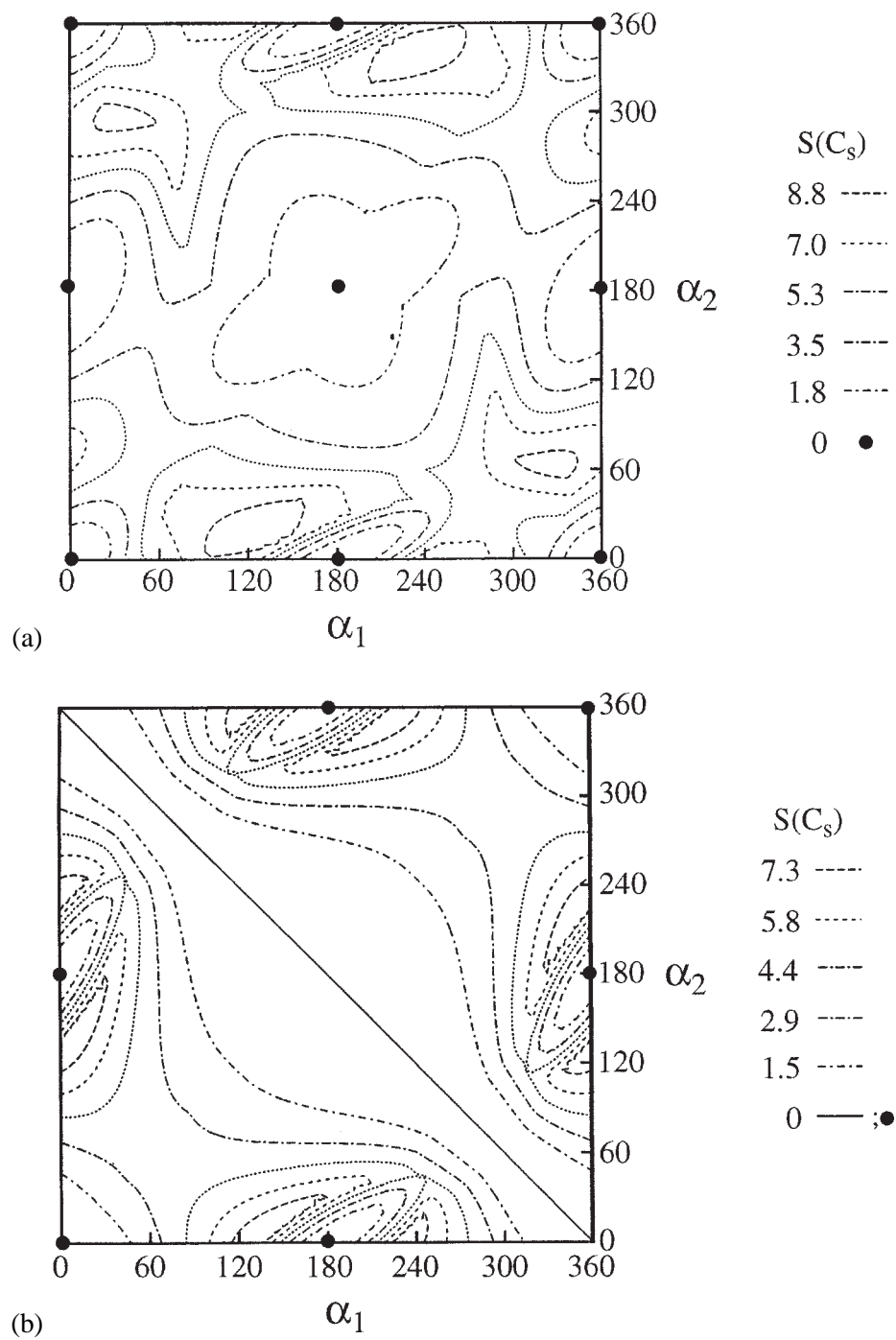
Figure 6. Chirality maps of butane stuctures with unequal bond-lengths. The bond-length ratios are:
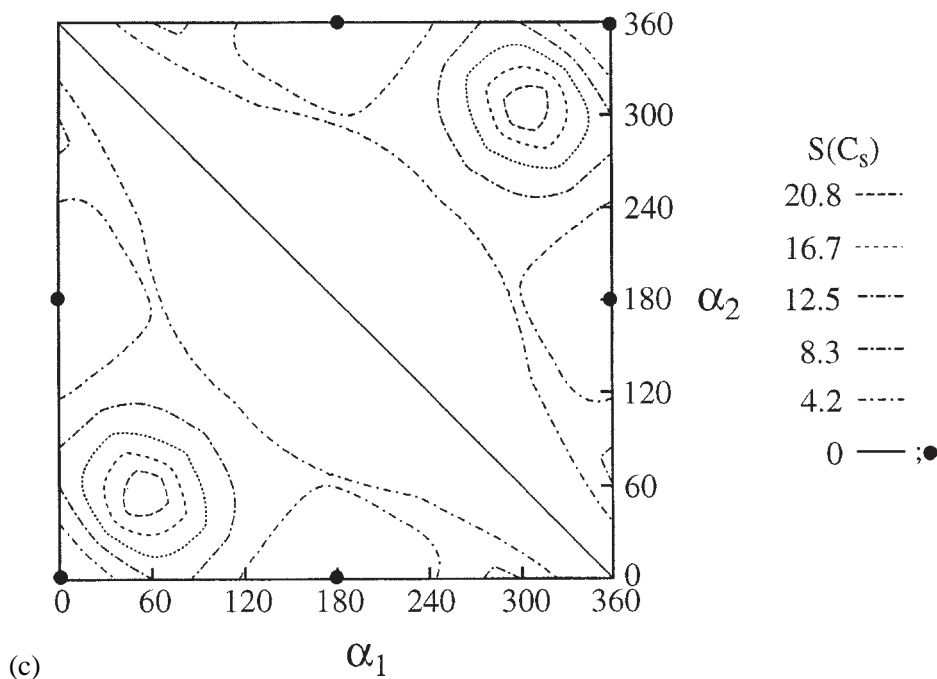(a) $1:1:2$; (b) $2:1:2$; (c) $1:2:1$.

Figure 6. (Continued.)

point groups; the map assumes a $C_s$ symmetry, if one of the axes is reversed). As explained earlier, any bent by $+\Delta\alpha_1$ has only one enantiomeric equivalent of $-\Delta\alpha_1$. The generalized chirality map (figure 6(a)) has only a few achiral points at $\alpha_1 = \alpha_2 = 180°$, $\alpha_1 = \alpha_2 = 0°$, $\alpha_1 = 0$, $\alpha_2 = 180°$ and at $\alpha_1 = 180$, $\alpha_2 = 0°$, where the butane structure has a 2D-$C_s$ symmetry.

The 2D-$D_2$ map symmetry encountered for the equal bond-lengths butane, is in fact obtained for all butanes of segment ratio $a : b : a$ (figure 6 (b) and (c)) for the same reasoning presented above. However, other features, such as the elevation, curvature and location of the non-differential lines (section 2.4 below), change. The chirality values here are lower than those of the equal bond length structure. The reason for it is that the longer the $P_2P_3$ bond is relative to the other two, the more the skeleton approaches an (achiral) line. Similarly, the shorter this bond becomes, the more the structure resembles a line for $\alpha_1 + \alpha_2 < 180°$ and an achiral $V$ structure for $\alpha_1 + \alpha_2 > 180°$. It turns out therefore that the equal lengths butane gives rise to the highest chirality values. The $\alpha_1 + \alpha_2 = 360°$ diagonal and the $\alpha_1 = 0$, $\alpha_2 = 180°$ and $\alpha_1 = 180$, $\alpha_2 = 0°$ dots are achiral in all $(a) : (b) : (a)$ butanes.

Finally, we note that the symmetry of the center point structure must dictate not only the symmetry of the chirality map but the symmetry of all maps of physical properties which are invariant to point and space symmetry operations (such as energy).

## 2.4. Non-differential points: Size normalization and "phase" maps of achirality

### 2.4.1. Size normalization

The use of $S(G)$ as a reaction coordinate may reveal non-differential points for which there are two sources. The first is due to the size normalization procedure. Our normalization factor has been the distance between the center of mass and the farthest point of the object. During a dynamic process, this vector may flip from one vertex to another, causing non-differentiability of the symmetry map. This type of discontinuity is technical, and can be removed without tampering with the essentials of the CSM and CCM algorithms. In order to achieve it we apply another normalization procedure, which has been commonly used as a shape-size normalization [4]: rather than dividing the points of the object by the farthest vertex distance, one divides it by root mean square (RMS) length of all the vectors in center of mass coordinates:

$$P_i = \frac{P_i^{\text{original}}}{\text{RMS}}, \tag{7}$$

where

$$\text{RMS} = \sqrt{\frac{\sum_{i=1}^{n} \|P_i^{\text{original}}\|^2}{n}}. \tag{8}$$

This normalization factor is smaller than the farthest vector normalization, because it weighs all distances, not only the longest. As a consequence, the chirality values in the RMS normalization are higher than in the farthest vertex method, although, as seen in figure 7 for the equal bond-lengths butane (compare with figure 5(a)), the *relative* value changes and most of the general trends and features within the paths, are preserved.[2] An example for the removal of discontinuity by changing the normalization procedure is shown in figure 8, in which figure 5(a) is reproduced. The diagonals (figure 8) divide the map into four sections of normalization behaviour: Across the $\alpha_1 = \alpha_2$ diagonal there is a flip between $P_1$ and $P_4$ as farthest vertices, and it is therefore a non-differentiable line in the map. This is also true for the other diagonal, however, this line links smoothly with its surroundings. The RMS normalization is devoid of this problem, and the $\alpha_1 = \alpha_2$ line links smoothly with its surroundings (figure 7, $\alpha_1 = \alpha_2$ diagonal not shown).

---

[2] In addition to solving the problem of non-differentiability, the RMS normalization has another advantage: using this method, if an object collapses into a single point after symmetrization, its symmetry value is 100, since

$$S(G) = \frac{100 \sum_{i=1}^{n} \|P_i^{\text{original}} - 0\|^2}{\left(\sqrt[n]{\left(\sum_{i=1}^{n} \|P_i^{\text{original}}\|^2\right)/n}\right)^2} = \frac{100n \sum_{i=1}^{n} \|P_i^{\text{original}}\|^2}{n \sum_{i=1}^{n} \|P_i^{\text{original}}\|^2} = 100.$$

This makes the CSM intuitive, unlike the value offered by the farthest vector normalization, the value in the latter method being $S(G) = 100 \sum_{i=1}^{n} \|P_i^{\text{original}}\|^2/(nP^{\text{farthest}})$. In this normalization method the value becomes 100 only if a perfect polygon collapses into a single point.
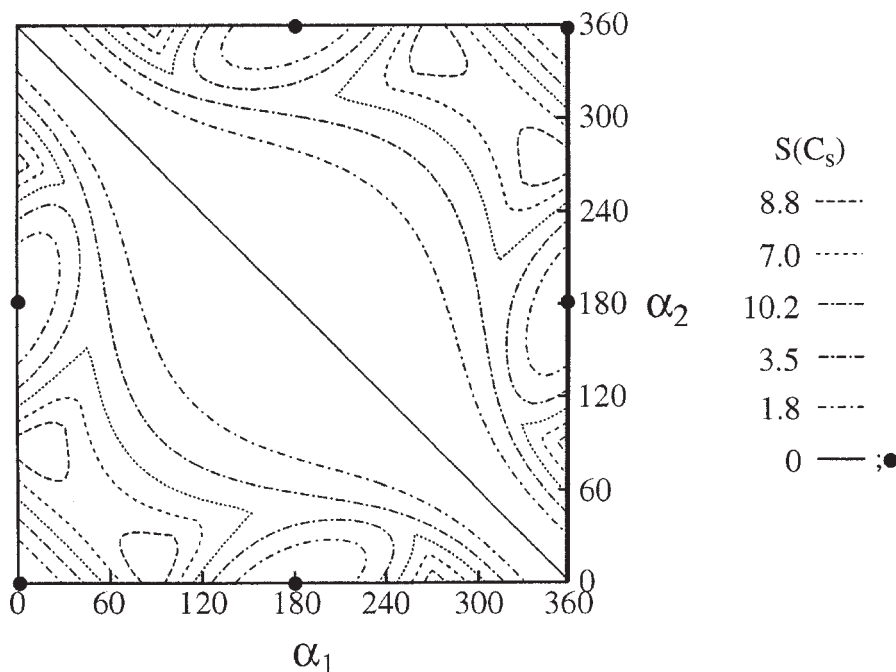
Figure 7. The effect of size normalization by the RMS method (all bonds equal). Compare with figure 5(a) where the normalization base used is the distance between the farthest vertex and the center of mass (see text).

### 2.4.2. Phase map of nearest achirality

The second source of non-differentiability is inherent to the search for the closest symmetric structure. If there are two or more different nearest types of shape for achirality, then the nearest achiral shape may jump with respect to a gradually changing chiral structure. This is in fact a jump of the vertices permutation during a dynamic process, namely, a change in the match of vertices that are reflected into each other in the nearest achiral structure. The change of the closest achiral structure occurs along the crossing line of two chirality value hypersurfaces, each belonging to a different achiral structure. A pathway leading from one hypersurface to the other is therefore non-differentiable at the point of passing the crossing line of these surfaces. This non-differentiability can be removed, if the restriction for nearest achirality is replaced with a restriction for a specific nearest achiral shape. This is a possibility we have yet to explore, although it gives up a central feature of the definition of the symmetry measure, namely that $S(G)$ is minimal. Here we make use of the permutation changes in the following way:

For butane there are, as we have already seen, two types of nearest achiral structures: a cisoidal one (permutation (1 4)(2 3) – figure 1(b)) and a linear one (permutation (1)(2)(3)(4) – figure 1(d)). These different nearest achiral shapes allow one to present and explore a corresponding *map of nearest achirality*. This map, which
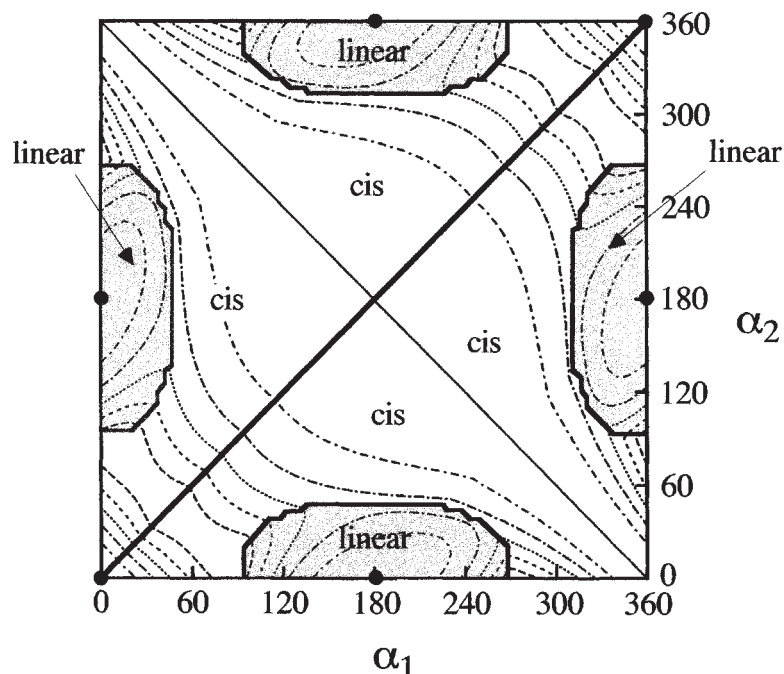
Figure 8. A "phase map" of the closest achiral structures of equal bond-lengths laid upon figure 5(a). The gray areas represent chiral structures whose nearest achirality is linear. The $\alpha_1 = \alpha_2$ diagonal represent structures that collapse after symmetrization to full spread ($D_2$) linear butanes. The border line between the "phases" is a non-differentiable ridge on the chirality map. The surface in figure 5(b) is the minimum of two surfaces – one corresponds to the distance to an achiral cisoidal structure and the other to the distance to a collinear one – their location is shown here. The diagonals divide the map into four equal segments of normalization in the farthest vertex method. At the top and bottom quarters, $P_4$ is farther from the center of mass than $P_1$. At the left and right parts, $P_1$ is farther.

resembles a "phase map" (figure 8), is laid upon the chirality contour map in fig-
ure 5(a) to show the relation between the two presentations. Because it is an equal
segment butane, there are three "phases" in this map: the shaded zones which cor-
respond to a full spread–full fold ($C_s$ linear closest achiral structure); the diagonal
line $\alpha_1 = \alpha_2$, which corresponds to a full spread–full spread or a full folded–full
folded ($D_2$) linear butane; and the non-shaded zones, in which the nearest achiral
shapes are cisoidal structures ($C_s$). This presentation shows that the 3D surface
(figure 5(b)) is indeed an interwoven blanket of two surfaces, each belonging to a
different nearest achiral type of structure. Indicating the crossing of two chirality
surfaces are the boundary lines around the linear-achirality islands (figure 8), which
are therefore non-differentiable. However, the structures represented by the $\alpha_1 = \alpha_2$
diagonal carry the two perpendicular mirror lines so they possess both the permutation
of the linear structures ((1)(2)(3)(4)) and that of the cisoid butane ((1 4)(2 3)). As
a consequence, the diagonal is a smooth zone on the RMS normalization chirality
map.

Finally, note that the symmetry of the phase map of nearest achirality is that of the chirality map itself; and that both normalization methods have the same phase maps of nearest achirality, since a division by a constant does not change the nature of the nearest achirality of an object.

## Acknowledgements

## References

[1]  D. Avnir, O. Katzenelson and H.Z. Hel-Or, Chem. Eur. J. (Angew. Chem. Int. Eng.) 2 (1996) 744.
[2]  D. Avnir, O. Katzenelson, S. Keinan, M. Pinsky, Y. Pinto, Y. Salomon and H.Z. Hel-Or, in: *Concepts in Chemistry: A Contemporary Challenge*, ed. D.H. Rouvray (Research Studies Press, Taunton, 1997) pp. 283–324.
[3]  V. Buch, E. Gershgoren, H.Z. Hel-Or and D. Avnir, Chem. Phys. Lett. 247 (1995) 149.
[4]  J.C. Gower, Psychometria 40 (1975) 33.
[5]  Y. Hel-Or, S. Peleg and D. Avnir, Langmuir 6 (1990) 1691; (Erratum: 10 (1994) 1633).
[6]  D.R. Kanis, J.S. Wong, T.J. Marks, M.A. Ratner, H. Zabrodsky, S. Keinan and D. Avnir, J. Phys. Chem. 99 (1995) 11 061.
[7]  O. Katzenelson, H.Z. Hel-Or and D. Avnir, Chem. Eur. J. 2 (1996) 147.
[8]  S. Keinan and D. Avnir, Presented at WATOC 96 in Jerusalem (1996); http://chem.ch.huji.ac.il/employee/avnir/watoc96/poster.html.
[9]  S. Keinan, H.Z. Hel-Or and D. Avnir, Enantiomer 1 (1996) 351.
[10]  P.G. Mezey, J. Math. Chem. 17 (1995) 185.
[11]  K. Mislow and R. Bolstad, J. Am. Chem. Soc. 77 (1955) 6712.
[12]  K. Mislow and P. Poggi-Corradini, J. Math. Chem. 13 (1993) 209.
[13]  Y. Pinto, P.W. Fowler, D. Mitchell and D. Avnir (1998, in preparation).
[14]  Y. Pinto, H.Z. Hel-Or and D. Avnir, J. Chem. Soc. Faraday Trans. 92 (1996) 2523.
[15]  L. Salem, Acc. Chem. Res. 4 (1971) 322.
[16]  V.I. Sokolov, in: *Introduction to Theoretical Stereochemistry* (Gordon & Bread, New York, 1991) pp. 75–76.
[17]  S. Wolfe, H.B. Schlegel, I.G. Csizmadia and F. Bernardi, J. Am. Chem. Soc. 97 (1975) 2020.
[18]  H. Zabrodsky and D. Avnir, Adv. Mol. Struct. Res. 1 (1995) 1.
[19]  H. Zabrodsky and D. Avnir, J. Am. Chem. Soc. 117 (1995) 462.
[20]  H. Zabrodsky, S. Peleg and D. Avnir, J. Am. Chem. Soc. 114 (1992) 7843.
[21]  H. Zabrodsky, S. Peleg and D. Avnir, J. Am. Chem. Soc. 115 (1993) 8278; (Erratum: 11,656).